

We are IntechOpen, the world's leading publisher of Open Access books Built by scientists, for scientists

5,800

Open access books available

142,000

International authors and editors

180M

Downloads

Our authors are among the

154

Countries delivered to

TOP 1%

most cited scientists

12.2%

Contributors from top 500 universities



WEB OF SCIENCE™

Selection of our books indexed in the Book Citation Index
in Web of Science™ Core Collection (BKCI)

Interested in publishing with us?
Contact book.department@intechopen.com

Numbers displayed above are based on latest data collected.
For more information visit www.intechopen.com



Additive Manufacturing of RF Waveguide Components

Mauro Lumia, Giuseppe Addamo, Oscar Antonio Peverini, Flaviana Calignano, Giuseppe Virone and Diego Manfredi

Abstract

The exponential growth of publications, in the last years, on the use of additive manufacturing (AM) technologies in the microwave field proves the increasing interest of research institutions and industries in these techniques. Some advantages of AM with respect to conventional machining are weight reduction, design flexibility, and integration of different functionalities (electromagnetic, thermal, and structural) in a single part. This chapter presents the most employed AM technologies for the manufacturing of RF waveguide components. First, an overview of the AM processes is discussed with particular care on material properties and post-processing. Then, an extensive survey on microwave-guided components fabricated by AM processes published in literature is shown.

Keywords: additive manufacturing, 3D printing, waveguide components, microwave components, SLM, SLA, FDM

1. Introduction

According to the American Society of Testing and Materials (ASTM), additive manufacturing (AM) is defined as “the process of joining materials to make objects from 3D model data, usually layer upon layer, as opposed to subtractive manufacturing methodologies.” Often this term is substituted by 3D Printing (3D Printing is typically associated with people printing at home or in the community; additive manufacturing is typically associated with production technologies and supply chains, but they both produce parts by the addition of layers). AM technologies can be classified into seven categories, namely, binder jetting, material jetting, direct energy deposition, sheet laminations, material extrusion, powder bed fusion, and vat photopolymerization. Each category includes several processes that share the same principle used for layer modeling and different materials that can be processed (**Table 1**).

AM has been first applied for rapid prototyping of visualization models and tooling. Recently, the improvement in the process’s accuracy and material properties of the manufactured objects have expanded the field of applications. Indeed, AM is currently used to manufacture personalized prostheses, replacement organs, and implants in the medical sector and produce complex lightweight components for the aerospace, automotive, and sports industries. Recently, AM has been applied by

Process	Technologies	Materials
Binder jetting	Ink-jetting 3D printing	Metal Polymer Ceramic
Material jetting	Polyjet Ink-jetting	Photopolymer Wax
Direct energy deposition	Direct Metal Deposition Electron Beam Direct Melting	Metal
Sheet laminations	Laminated Object Manufacture Ultrasonic Consolidation	Metal Polymer Ceramic Paper
Material extrusion	Fused Deposition Modeling	Polymer
Powder bed fusion	Selective Laser Sintering Selective Laser Melting Electron Beam Melting	Metal Polymer Ceramic
Vat-photopolymerization	Stereolithography Digital Light Processing	Photopolymer Ceramic

Table 1.
Seven categories of AM technologies [1].

RF industries for the development of next generations of microwave and millimeter-wave components for sensors, imaging systems, and satellite communication (SATCOM) [1].

A generic AM process starts with a model generated using a three-dimensional Computer-Aided Design (3D CAD) system. Then the model is converted into the STL file format that approximates the 3D model with a mesh of triangles. Then, this file is transferred to the AM machine to set the process parameters. Such settings are defined according to the geometry of the model (e.g., position and orientation of the components, design of support structures) and to the building process (e.g., energy source, material constraints, and layer thickness). At the end of the printing process, the part is removed from the building platform and prepared for the post-processing operations, for example, cleaning, sandblasting or shot-peening, thermal treatments, and plating [2].

The main advantage of AM process is manufacturing lightweight components with complex internal surfaces in a single part. Moreover, by eliminating tools, the design flexibility is increased. On the other hand, the main concerns are the manufacturing accuracy and the surface roughness that are worse than standard manufacturing processes and strongly depend on the material and process parameters.

In the microwave area, Selective Laser Melting (SLM)¹, Stereolithography (SLA), and Fused Deposition Modeling (FDMTM) are the most investigated technologies. The application of AM processes in manufacturing microwave and millimeter-wave components strictly depends on the accuracy, cost, and performance requirements. From this point of view, basic knowledge of the characteristics of a single process is necessary. This overview is reported in Sections 2–4. Section 5 is, instead, devoted to giving a survey of the principal results (in terms of realized components) actually achieved in the specialized literature. In this summary, all the important aspects for microwave

¹ The process Selective Laser Melting is, nowadays, sometimes called Laser Powder Bed Fusion (LPBF).

engineering are reported, i.e., operative band, measured results versus the expected ones, and an explanation of this difference. This section is split into subsections for reader convenience according to the component category.

2. Selective laser melting

SLM is an AM process that allows the manufacturing of all metal parts. This technology can easily realize complex geometries with interior features and channels. Regarding **Figure 1**, the manufacturing process starts with a thin layer of metal powder spread by a recoater along with the building platform. Then, a high-energy laser beam selectively fuses the deposited powder layer. The laser follows the contour defined in the STL file. Once a layer is completed, the building platform is lowered, the new powder is spread, and the laser melts this new layer. The process is repeated until the parts are completely manufactured. Due to the high temperatures necessary for melting, the process takes place in a protected atmosphere, normally argon, to prevent oxidation of the parts [1]. At the end of the process, the excess powder is removed; the parts still attached to the building platform undergo a stress-relieving job in an oven. This thermal treatment is necessary to reduce deformations of the parts caused by the high thermal stresses arising during the manufacturing process. Finally, the components are detached from the building platform and eventually subjected to surface finish treatment as polishing and shot peening [3].

Metal powder properties are important in the final quality and cost of the part built via SLM. The main properties influencing the process can be subdivided into three categories, which are as follows: [4]:

- geometrical (size and shape);
- metallurgical (microstructure, composition);
- mechanical/physical (flowability, absorption of light).

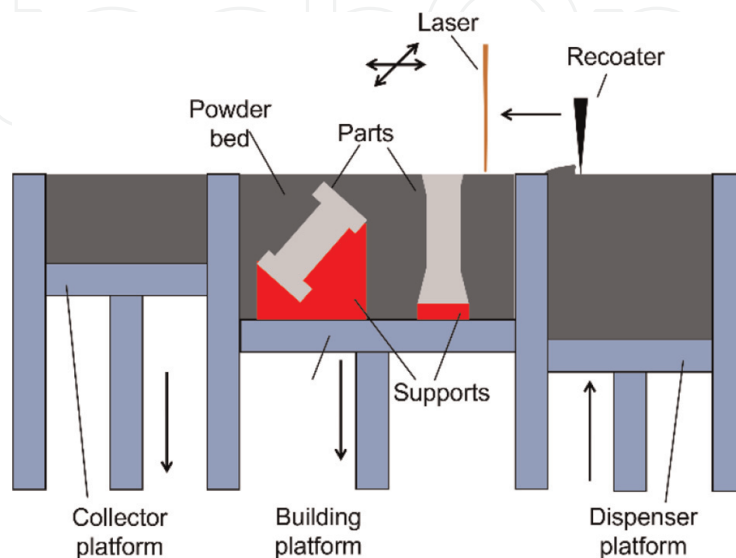


Figure 1.
Selective laser melting process.

As far as the first point is concerned, fine particles enable high-density parts with good surface quality, while the spherical shape improves flowability and, hence, mechanical properties [5]. Irregular powder particles can lead to poor surface finish, low density, and increased defects [6].

Extremely important steps in the SLM process are the orientation of the part in the building platform and the design of the supporting structures. Supports have mainly three purposes, which are as follows:

- to fix the part to the building platform;
- to conduct excess heat away;
- to prevent deformation or collapse of the part.

Typical drawbacks are as follows:

- an increment of the building and the post-processing time;
- their removal is not, in general, an easy task, and the risk of damage is quite high.

A possible solution to reduce the number of supports consists of choosing an optimal building orientation. It is worth noticing that the staircase effect has to be also well-considered for specific applications. The generation of the staircase effect is described in **Figure 2**. The STL file format is a triangular approximation of the nominal CAD. If the layer thickness is too high or the inclination angle is too small, the staircase effect becomes more remarkable. On the other hand, overhanging surfaces is another important aspect to consider. These surfaces are areas not supported by solidified material during the building process. The heat-conduction rate of powder-supported zones is lower than the solid-supported zones, while the absorbed energy is higher. The melt pool created by the laser becomes too large and sinks into the powder. Therefore,

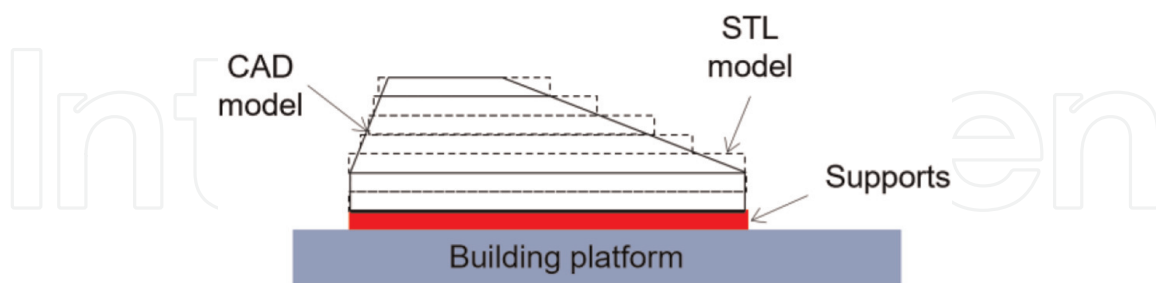


Figure 2.
Generation of the staircase effect.

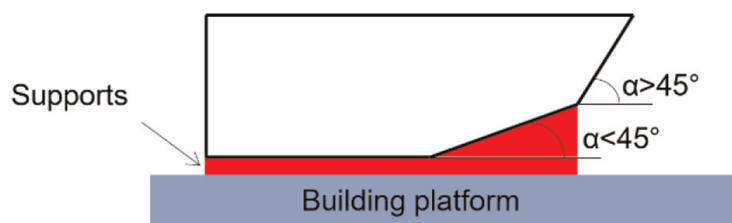


Figure 3.
Self-supporting angles.

deformation occurs if these surfaces are not supported. Supporting structures are usually built with a low density during the manufacturing of the part, and they must be manually removed at the end of the manufacturing process. A clever solution is represented by self-supporting angles (**Figure 3**). Based on experimental results, downward sloping faces with angles $\alpha > 45^\circ$ are self-supporting. At the same time, staircase effects can be reduced by increasing sloping angles. Moreover, in this way, the value of surface roughness decreases. On the contrary, angles lower than 30° should quickly be avoided since the staircase effect increases [7].

Materials commonly used in the SLM process are aluminum alloys, titanium alloys, stainless steel, Ni-based alloys, and cobalt-chromium alloys [1]. From an RF point of view, the most interesting ones are the aluminum ones as the AlSi10Mg alloy. This material exhibits high electrical conductivity, low-specific weight, high corrosion resistance, and good mechanical properties. The typical achievable accuracy guaranteed for this aluminum alloy is in the order of ± 0.1 mm [3]. However, better manufacturing accuracy has been observed in literature for components designed with an AM-oriented approach.

3. Stereolithography

Stereolithography (SLA) was developed in 1984 by Charles Hull and was the first available commercial AM process. SLA is a vat photopolymerization process based on the solidification of a liquid resin using a UV laser. Since the process takes place in a liquid, support structures are necessary during the building phase. These are made by the same material of the parts and are specified in the machine parameter settings [1].

Concerning **Figure 4**, the manufacturing process starts with the building platform lowered from the top of the vat by a layer thickness. Then, a recoater blade smooths the surface of the vat, and a UV laser cures the material. Then, the platform is lowered by a layer thickness, and the process is repeated until the part is completed. At the end of the process, the platform is lifted, the part is drained and removed from the platform [8]. Then, it is placed in a UV oven to complete the curing. During the solidification process,

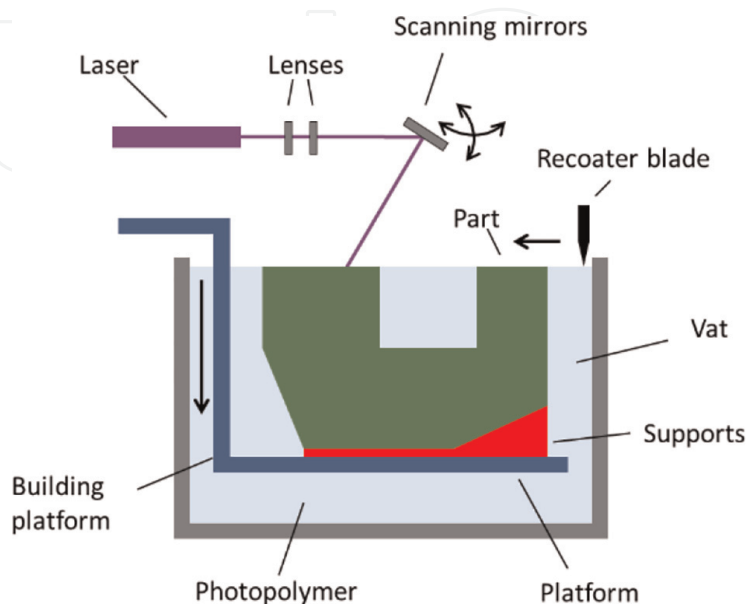


Figure 4.
Stereolithography process.

usually, the photopolymer shrinks. This shrinkage induces compression stresses on the previous layers that may cause curling and distortion. These effects can be reduced by adopting clever scan strategies, such as Star Weave or ACES [1].

Acrylates resins were the first photopolymers developed. These resins had high reactivity but produced inaccurate parts due to a significant shrinkage (5–20%) and a tendency to warp and curl. They are low viscosity resins used for visual or anatomic models, with a low accuracy but high-speed manufacturing. On the contrary, epoxy resins present high viscosity and are used for functional parts. They have slow photo speed but allow more accurate, harder, and stronger parts than the acrylate ones.

Furthermore, they exhibit low levels of shrinkage (1–2%), reducing the risk of warp and curl. Most of the commercially available resins are epoxides with acrylate content to combine the advantages of both materials [2]. Moreover, it is possible to suspend ceramic particles in a resin to obtain a ceramic–polymer composite material and improve mechanical and thermal properties.

SLA allows the manufacturing of parts with good accuracy ranges from 25 to 50 μm and smooth surfaces; the typical average surface roughness R_a is lower than 10 μm . However, the metal plating of the internal channels can be critical in terms of adhesion, uniformity of the metal coating, and long-term stability [9], limiting the applicability of SLA in the manufacturing of some RF applications (e.g., waveguide components for space).

4. Fused deposition modeling

FDM, also known as Fused Filament Fabrication (FFF), is a material extrusion process in which material is heated and then dispensed through a nozzle layer by layer. The process was invented and patented by Scott Trump in 1989, who then founded Stratasys Inc. The basic process is based on a robot arm that moves two nozzles where a filament of polymeric material is fused and then deposited layer by layer on a platform (Figure 5). The filament is supplied by an unrolled spool and

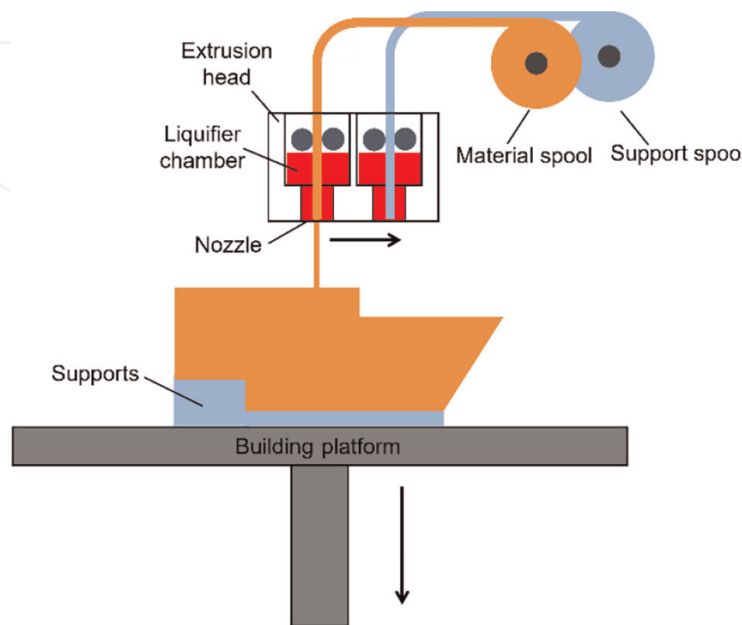


Figure 5.
FDM process.

pressed into the extrusion head. The material is then heated utilizing electrical resistance [1]. Heat is conducted to the liquefier chamber to obtain a liquid state. The material inside the chamber should be maintained in a molten state, with particular care on the temperature since some polymers degrade at high temperatures and could burn [2]. The filament is softened, the molten material gets off through a nozzle of reduced diameter and deposits on the building platform [1].

The nozzle diameter determines both the shape and size of the extruded filament and the minimum feature size that can be printed—the larger the nozzle diameter, the faster the process, but with lower precision. Material extrusion is controlled by the pressure difference between the chamber and the atmosphere. If the pressure is maintained constantly, the material flows at a constant rate with a constant cross section. The same happens if the nozzle speed is kept constant. Any change in the direction of the extrusion head must result in a change in the corresponding material flow rate. Otherwise, a different amount of material will be deposited in that region. Once the material is extruded, gravity and surface tension can cause a change in the shape, while the cooling and drying effects can change the size of the material deposited. This effect can be reduced by minimizing the differential temperature between the chamber and the atmosphere. Bonding with the previous layer and the adjacent region can be ensured by residual heat energy or solvents and wetting agents in the extruded filament [2].

FDM machines can be equipped with one to three nozzles. In this case, two nozzles deposit two different building materials, while the third one is filled with a soluble material for supporting structures. The former case is employed for a low-cost solution for large industrial machines. In this way, the support material is not removed manually but is dissolved in a chemical bath after the fabrication process.

Many thermoplastic materials are available for FDM and FFF processes; the most commonly used for RF applications are listed below [1].

- Acrylonitrile Butadiene Styrene (ABS) is a generic thermoplastic material used in injection molding processes. The main properties are hardness, strength, and heat resistance. Companies developed different kinds of ABS, each with specific properties, and many colors are available for FDM printers. ABS exhibits good adhesion so that it can be used with high printing speed.
- PolyLactic Acid (PLA) is a common biodegradable plastic obtained from corn or sugar cane. It is used for shopping bags and packaging, but it can also be used for biocompatible medical implants. PLA is one of the materials most used for low-cost printers because of its environmental sustainability. However, it is not ideal for high-temperature environments or outdoor applications. Like ABS, different colors and different types of PLA are available. PLA exhibits good adhesion so that it can be used with high printing speed
- Polycarbonate (PC) is a polymer with good temperature resistance and high impact resistance. However, PC is very hygroscopic and absorbs moisture from the air. Moreover, it must be used with a heated bed to avoid warping problems. PC is available in black or transparent colors.
- Polyamide (PA) is commonly known as Nylon. PA is the most common nylon material used in FDM printers because it has good strength, a low-friction coefficient, and can take up vibrations or impacts. However, it tends to warp

more than ABS and PLA. For this reason, the use of a heated building volume is recommended.

- ULTEM is a thermoplastic material developed by Saudic and commercialized by Stratasys. It has high heat and chemical resistance, good strength, flexibility, and impact resistance. It is used for aerospace and medical parts.
- PEEK is an organic thermoplastic material developed by Victrex. It has high heat and chemical resistance and good strength. It is a biocompatible material used for manufacturing medical, aerospace, and automotive parts.

FDM allows the manufacturing of multi-material parts. The use of a soluble support material offers good design flexibility. The main concern with this technology is that the nozzle dimensions limit the accuracy. The typical resolution of the process is about 100–200 μm . As in the case of SLA, a metal plating of the internal channels is mandatory for waveguide RF application.

5. RF applications

The manufacturing of RF components by AM process is particularly challenging for different reasons. The internal channels of the parts have to be designed considering the typical AM post-processing operations, for example, powder removal in SLM or metal plating in SLA and FDM. Moreover, due to the typical accuracy of the AM processes, an electromagnetic robust design approach is mandatory in the case of high RF-performance components.

The simplest strategy consists of splitting the component into two or more parts. This way is usually employed in the case of SLA and FDM to ease electroless metal plating processes. Sometimes this is also used in SLM products, particularly for complex internal structures. The main drawback is misaligning the different parts with consequent leakage effect and, subsequently, higher losses. Moreover, the intrinsic features of AM processes are not employed, making their employment, therefore, less effective and convenient.

The designed part should be realized monolithically to take full advantage of the AM process. To achieve this goal, the electromagnetic design has to be adapted to the process in a so-called “*AM-oriented design*.” The most important is aligning the propagation axis with the building direction, avoiding, at the same time, the presence of overhanging structure in the internal channel (for instance, stubs or corrugations). These criteria, then, force a complete reconsideration of well-known RF structures. One of the main advantages is better manufacturing accuracy and symmetry of the cross section (essential characteristic for dual-polarization components).

The following subsections summarize the most common 3D-printed RF components, namely—waveguides, filters, horn antennas, dual-polarization components (OMTs and septum polarizers). Finally, the last subsection describes some examples of the integration of different RF functionalities into a single component.

5.1 Waveguides

Waveguide lines are the simplest candidates for evaluating the best achievable accuracy of the AM technologies for microwave components. An important

parameter is the realized metal loss per wavelength/cm. Different factors influence these values:

- the material conductivity;
- the surface roughness;
- the dimensional accuracy;

Deep research has been done considering different AM technologies and a frequency range that spans from Ku- to E- band (10–170 GHz). A summary of these works with relevant results is reported in **Table 2**. As observed, SLM and SLA are the most commonly exploited technologies since they ensure good accuracy and low roughness compared to other AM processes.

Going more into detail, an interesting example of a waveguide manufactured by FDM is reported in ref. [10]. Firstly, a WR42 waveguide has been printed using ABS. Then, the same printer was customized to deposit a low-cost conductive silver ink. The manufactured waveguide exhibits a measured loss of 0.11 dB/cm for the entire K-band.

As far as the SLA is concerned, mainly the W- and D-band (75–170 GHz) have been considered. In Refs. [11–13], the copper plating has been applied, showing a W-band loss mean value of 0.06 dB/cm. An interesting comparison between commercial and SLA waveguides is reported in [12], showing that SLA components present a measured loss that is almost double of the commercial ones: 0.06 dB/cm versus 0.03 dB/cm and 0.26 dB/cm and 0.15 dB/cm in W- and D-band, respectively.

As far as the SLM is concerned, the main test refers to the frequency range from 18 to 110 GHz. Aluminum is the material most used. However, few examples have been carried out by using copper and nickel alloys [11]. An interesting comparison is presented in Ref. [11], where the authors compare the losses of a commercial WR42 waveguide with SLM (in aluminum) and a CNC machined realization. As it could be expected, the lowest attenuation occurs in the commercial waveguide (0.004 dB/cm), while the SLM and CNC parts exhibit a loss of about 0.02 dB/cm and 0.03 dB/cm, respectively. Still considering SLM, in Ref. [15], a study on the circular waveguide,

Ref.	Frequency (GHz)	Waveguide	Technology	Material	Loss (dB/cm)
[10]	18–26	WR42	FDM	Silver plated	0.11
[14]	18–26	WR42	SLM	AlSi10Mg	0.02
[15]	26–38	Circular	SLM	AlSi10Mg	0.01
[11]	75–110	WR10	SLM	GRCOP-84	0.141
				Inconel 625	0.369
				AlSi10Mg	0.103
[12]	75–110	WR10	SLA	Copper plated	0.055
[12]	75–110	WR10	SLA (DLP)	Copper plated	0.063
[13]	75–110	WR10	SLA	Copper plated	0.06
[12]	120–170	WR6	SLA (DLP)	Copper plated	0.26

Table 2.
 Losses of AM waveguides.

operating in Ka-band, is carried out. The measured aluminum prototypes exhibit a loss of 0.01 dB/cm. The co-polar and cross-polar transmission coefficients have been measured to understand the SLM's feasibility for dual-polarization systems, thanks to the double symmetry shape. The measurements show a spurious cross-polarization term of -25 dB/ -40 dB.

A comparison, in W-band, between parts SLM realized with different alloys (aluminum, copper, and nickel alloys) is reported in Ref. [11], showing the better behavior of the aluminum prototype.

5.2 Waveguide filters

Filters are one of the most demanding elements from a manufacturing point of view. The high-standing waves developing inside the components lead to high sensitivity to mechanical tolerances and high susceptibility to multifactor discharge and passive intermodulation products (PIM). For this reason, they are an important benchmark for the AM manufacturing of passive waveguide components [3].

A detailed review of 3D-printed microwave filters has been recently reported [16]. The frequency range considered in literature is mainly 7–22 GHz, although a few examples at higher frequency bands (up to 110 GHz) have also been discussed. Metal, plastic, and ceramic materials have been employed in published works.

FDM has been used in Ref. [17] to manufacture two X-band filters with PLA filament. Each component has been manufactured in two halves with an E-plane cut. The parts are coated with a copper spray to create a conductive surface for the galvanization process with further copper. Despite the accuracy of the printing and painting process, good results have been obtained for both filters. In Ref. [18], a two-pole X-band filter in the WR90 waveguide insert has been manufactured using PC filament. The printed insert has been coated with a nickel spray and then electroplated with copper.

As far as the SLA process is concerned, in Ref. [19], a four-pole quasi-elliptic filter, working at $810 \text{ MHz} \pm 16 \text{ MHz}$, is presented. The filter is composed of two mushroom-shaped resonators. The filter has been realized in two blocks, metalized with silver painting and then electroplated with copper. The same manufacturing approach has been reported in Ref. [20] for a two-pole filter.

Considering SLM realizations, an example of a W-band filter is presented in Ref. [21]. The filter is based on five rectangular resonators coupled using inductive irises. Two stainless steel prototypes have been manufactured, one coated with $5 \mu\text{m}$ of copper showing different measured electrical conductivity: $1.25 \times 10^7 \text{ S/m}$ and $5.96 \times 10^7 \text{ S/m}$, respectively. As far as, the scattering parameters are concerned, the stainless steel filter shows a center frequency shift down by 1.66 GHz and a minimum return loss of 24.41 dB in the passband, while the copper-plated presents a frequency shift of 0.9 GHz with a return loss is 26.56 dB.

Some examples of monolithic realization and comparison between materials and processes are reported in Refs. [9, 22]. In Ref. [9], a comparison for Ku/K filter prototypes realized both in SLM (in aluminum, titanium, and maraging steel alloys) and SLA (copper plated) is shown. The study proves that an AM-oriented architecture provides excellent results in both roughness and mechanical accuracy; at the same time, the metallization of the SLA component is extremely complicated in the inner surfaces of the filter. A similar comparison is reported in Ref. [22], where two prototypes, operating in X-band, have been manufactured—one by SLM with an aluminum-copper alloy, the other by SLA, and then copper electroplated. The most

interesting contribution of this paper was the excellent performance, even for the SLA filter.

Ceramic materials have also been used for the 3D printing of waveguide filters with two different approaches. The first method consists of manufacturing ceramic components, subsequently, metal plating. For example, in Ref. [23], a ceramic-filled resin has manufactured hemispherical resonator waveguide filters. Four Ka-band filters have been manufactured, metal plated, and measured with good RF results. The electroless plating process consists of a deposition of palladium, nickel, and copper, followed by a passivation layer of silver. In the second approach, the materials' dielectric properties are exploited to reduce the overall envelope.

For instance, Ref. [24] manufactured a dielectric perturber for a third-order filter with a bandpass shifting from 10 to 12 GHz. The filter was manufactured using copper with a standard manufacturing process, while the perturber was manufactured by SLA using zirconia ($\epsilon_r = 32$, $\tan \delta = 0.002$). In Ref. [25], the authors used alumina ($\epsilon_r = 9.1$, $\tan \delta = 0.0001$) to manufacture the dielectric resonators in a sixth-order quasi-elliptic bandpass filter. The housing has been 3D printing in two blocks using plastic material and then metal plated. An important aspect of this work is that no supports or glue are needed. The dielectric resonators are placed in the middle of their cavities to maximize their Q-factor.

5.3 Horn antennas

Waveguide horns are commonly used in high-performance antenna feed chains in SATCOM applications. This class of antennas, indeed, can provide excellent performances in terms of gain, bandwidth, return loss, and cross-polarization [26]. Therefore, much effort has been made to study the 3D printing of waveguide horns. Most of the works are from X-band to K-band (7–27 GHz), although some examples can be found up to 300 GHz [27].

As far as the SLA process is concerned, three works are particularly interesting. In the first one [28], a 2–12 GHz double-ridge horn antenna is presented. The internal surface has been coated with a layer of silver ink with a conductivity of 4×10^5 S/m.

In Ref. [29], a comparison between SLA and standard process (lathe in aluminum) has been considered to realize a spline horn operating in the Ku-band. Both prototypes exhibit good agreement between the simulated and measured value of the co-polar pattern, while worse performances in terms of losses and cross-polarization level can be noticed in the AM one. The latter is mainly related to the higher surface roughness, which has been estimated equal to $1.79 \mu\text{m}$. In Ref. [30], a metal-plated 240 GHz choke horn antenna has been reported. The antenna has been designed to obtain 12 dBi gain from 200 to 280 GHz. The measured radiation pattern is in good agreement with the simulation.

Considering the SLM process, six works are particularly significant [26, 27, 31–34]. The first four refer to the manufacturing of classical architecture to understand the applicability of the SLM technique. The last two show some interesting work in the exploration of AM features.

In Ref. [26], the manufacturing of three smooth-wall horns, working in Ku-, Ku/K-band, and Q/V-band, is presented. The smooth-wall design allows the alignment of the building direction with the propagation axis, ensuring a good cross-sectional symmetry and low cross-polarization level. The horns have been manufactured using aluminum alloy. All the antennas exhibit good agreements between measured and simulated values. In particular, return-loss higher than 33 dB, cross-polarization lower

than -28 dB, and peak gain of 25 dBi have been obtained. Moreover, a 3D scan of the outer section of the horns reveals an accuracy between 0.06–0.08 mm.

In Ref. [27], the manufacturing of 300 GHz corrugated horn antennas. Four prototypes have been manufactured using a tin-bronze alloy with an electrical conductivity of 7 MS/m. The dimensions of the prototypes differ by 5% with respect to the theoretical model. Nevertheless, the measurement results have observed good symmetry between E-plane and H-plane. However, the antenna efficiency is relatively low due to the conductivity of the material used in manufacturing. To improve the RF performances, all the prototypes have been plated with 3 μm of gold (conductivity of 44 MS/m).

In Ref. [31], an X/Ku-band (8–18 GHz) choked horn SLM manufactured in the aluminum alloy is presented. To investigate process manufacturing accuracy and repeatability, 15 prototypes have been manufactured, showing an overall accuracy of 0.1–0.3 mm and a roughness Ra of 3.5 μm . The feeding gap and the radiating aperture have been milled after the manufacturing process, with an accuracy of ± 0.02 mm.

In Ref. [32], a Ku-band spline horns SLM manufactured in aluminum and titanium alloys are presented. The manufactured components' roughness is about 16 μm for both the materials, but it reduces to 3.4 μm for the Al one after the post-processing. The radiation pattern of the two prototypes is in good correlation with the simulation, but the titanium horn exhibits a worse cross-polarization level due to a slight ellipticity of the aperture. In the same paper, the manufacturing of a cluster of four spline horns is presented, showing a mass reduction of 30% with respect to classical manufacturing.

In Ref. [33], a perforated X-band (8–12GHz) horn antenna has been presented to lighten the component. The holes' dimensions are lower than 1/15th of the wavelength at 12 GHz. Not considering the SMA connector, the antenna weight is just 8 g. The good agreement between simulated and measured RF results demonstrates an efficient method to reduce weight without affecting performance. A similar idea has been applied in Ref. [34] for a steel pyramidal horn antenna.

FDM process has been used to manufacture waveguide horns up to 15 GHz. In Ref. [35], the authors presented the first additively manufactured dielectric-loaded profiled conical horn antenna in the frequency range from 9 to 15 GHz. The component has been manufactured using polylactic acid (PLA) with relative permittivity $\epsilon_r = 2.72$. Two concentric dielectric cores with different infill factors have been printed to obtain the desired relative permittivity inside the horn. After the manufacturing process, the outer surfaces of the horn have been plated with 10 μm of copper. Surface roughness of 8.050 μm has been measured after the plating process. The measured radiation pattern is in good agreement with the simulation, with a cross-polarization level less than -21 dB up to 13 GHz. A measured S11 lower than -10 dB has been obtained from 10 to 14 GHz. The antenna exhibits a gain of 16.0–20.0 dBi and total efficiency of 60–91% over the frequency range from 9 to 15 GHz. In Ref. [36], three X-Ku pyramidal horn antennas have been 3D printed using ABS material and then metal plated using copper or chromium and nickel, respectively. As expected, the copper prototype exhibits the best performance.

5.4 Dual-polarization components

Orthomode transducers (OMT) and septum polarizers are classical components used in dual-polarization antenna feed-chain systems. Separate the two linear polarization of

the incoming signal routing them to two different rectangular waveguides [37]. Septum polarizers are employed to route the two circular polarizations in the common waveguide (typically circular or square) to the TE₁₀ modes in two different rectangular waveguides and vice versa. The most important parameters are insertion loss, isolation between the rectangular ports, and cross-polarization in transmission [38].

Starting with SLM realizations, a C-band septum polarizer operating in the frequency band 3.6–4.4 GHz is shown in Ref. [39]. The component has been manufactured of Scalmalloy® with a measured dimensional error of 0.6 mm. The return loss is better than 25 dB and the isolation greater than 23 dB, while the deviation between measured and simulated axial ratio is about 1 dB mainly caused by a not perfectly circular common section. Moving up in frequency, in Ref. [40], two single sidearm OMTs are presented. The components are designed in the frequency band 10–15 GHz. The two OMTs have been compared with a realization by conventional manufacturing techniques. In this work, the OMT geometry realized was not figured out for AM process.

Nevertheless, both components exhibit RF performances in good accordance with the traditionally machined components. An example of an OMT realization of an AM-oriented geometry is reported in Ref. [41], where the RF measured performances well match the simulated one. Isolation over 50 dB and return loss better than 20 dB have been achieved in the operative frequency range. Considering the Ka-band, an asymmetric side-coupling OMT has been presented in Ref. [37]. The OMT geometry has been conceived to be AM-oriented by using a multi-slope junction. The manufactured prototype exhibits good accordance with measured and simulated RF results. In particular, the insertion loss is lower than 0.25 dB, and the return loss is better than 27 dB. Then, in Ref. [42], the OMT design has been integrated with a twist in the coupled arm. The measured results are in good agreement with the simulation. In particular, the return loss for both polarizations is better than 27 dB, and the insertion loss is lower than 0.15 dB and 0.2 dB for the inline and coupled channels, respectively, which corresponds to an equivalent resistivity of 16 $\mu\Omega\text{cm}$. The prototype has been controlled by a computer tomography scanner showing a mechanical accuracy in the range 0.02–0.04 mm.

By considering the SLA process, in Ref. [43], a V-Band (50–75 GHz) OMT manufactured is presented. The OMT has been metal plated with a process developed by SWISSto12. This consists of copper plating and passivation using a thin layer of gold or silver. The novelty of this OMT is the multi-step conical post on the turnstile junction. This permits easy printing by SLA.

Septum polarizers have also been realized. In Ref. [38], a Ka-band prototype realized in SLM is presented. Two 45° bends have been integrated to accommodate standard WR28 flanges. The device has been designed to align the propagation axis with the building direction to guarantee the best cross-sectional symmetry. Thanks to this choice, the measured cross-polarization level is better than 30 dB and the isolation better than 28 dB.

In Ref. [44], a broadband septum polarizer has been manufactured in SLA and copper plated. The paper shows a novel design with a triangular common port design that allows a higher bandwidth than circular or square waveguide polarizers. The polarizer has been firstly designed in W-band and manufactured with a standard machining process. Then, the design was scaled in K-band and manufactured with an SLA printer. The prototype has been coated with conductive ink and then subjected to galvanic copper plating. Both the components exhibit isolation greater than 17 dB and a return loss better than 14 dB over 37.8% of bandwidth. Moreover, the insertion loss is lower than 0.4 dB for the 3D-printed prototype.

5.5 Integrated components

As reported in Ref. [40], one of the main advantages of the AM technologies is the free shape feature that can lead to an additional degree of freedom in the design of RF components, for instance, the integration of different functionalities (electromagnetic, mechanical, and thermal) in a monolithic component [45].

The previous survey has shown the evolution of the employment of AM process in the realization of guided microwave components, improving the quality of the realized parts, but this potentiality of AM is still not fully explored. A survey of some interesting and successful examples of this initial work is reported.

In Ref. [46], a mono-block Ku-band front-end, a combination of two integrated sub-assembly, a diplexer, and a 2×2 horn antenna array, has been presented. The components have been manufactured using the SLA technology and metalized with copper and tin with an electrolytic process. Measurement results agree with the simulated performances with a frequency shift of 150 MHz that can be related to the thickness of the metal deposition, not considered during the design.

In Ref. [38], a Ka-band feed horn integrated with a septum polarizer, manufactured with the SLM process using aluminum alloy. The septum polarizer, presented in the previous section, has been integrated with a smooth-wall horn. The measured values of return loss, cross-polarization, and isolation are comparable with the results of the septum polarizer alone, namely a return loss better than 25 dB, an isolation between the rectangular waveguide higher than 27 dB, and a cross-polarization better than 28 dB. The measurement results are comparable with those obtained with a standard manufacturing process in a split block layout.

In Ref. [47], an interesting study of an integrated feed system working in the frequency band in X-band (from 7.2 to 8.2 GHz) is presented. The device is composed of a circular horn antenna and an OMT. The authors compare the 3D printing of the feed system as a mono-block with the manufacturing in two symmetric pieces. Both the components have been printed using SLA and copper plated with a three-step metallization process. Although the two-pieces prototype has the advantages of an easier manufacturing process and the thickest metal coating, the monolithic component exhibits better RF performances.

A similar component has been developed and presented in Ref. [48]. The integrated Ku-band feed chain consists of a spline horn and an OMT and has been manufactured using the SLM process. The RF performances are compared with those obtained with standard machining processes. An X-band feed chain has been presented in the same paper. The developed component consists of a spline horn and a compact E-plane waveguide coupler. The feed chain is three times lighter than a comparable, conventional manufactured component. Perfect agreement with the simulated performance has also been obtained with these components.

In Ref. [49], an entire Ku-band feed cluster manufactured by SLM technology, suitable for SFB scenarios, is presented. The feed cluster operates in Tx- and Rx-frequency bands. The component consists of 18 feed chains composed of a horn, a transition, a single sidearm OMT and waveguide routing to provide interfaces for the measurement. The scattering parameters have been measured for both the frequency bands showing a return loss better than 19.5 dB and the isolation below -50 dB. The feed cluster exhibits excellent agreement between simulated and measured values of the pattern at 11.30 and 14–25 GHz.

In Ref. [50], a high gain K-band feed chain has been manufactured by SLM using aluminum alloy. The measurement results show return loss and port-to-port isolation better than 23 dB. The axial ratio is between 0.1 and 0.5 dB, while the cross-polar discrimination (XPD) is better than 30 dB. The measurements show good manufacturing accuracy with good rotational symmetry.

In Ref. [51], a passive front end for satellite communication, manufactured by SLM technology using aluminum alloy, is discussed. The component comprises four conical horns, four rectangular-to-circular waveguide tapers, two-stage 1×4 power dividers, and a WR-42 waveguide interface. The scattering parameters have been measured in the frequency band 19–21 GHz. Discrepancies between simulated and measured RF performances have been observed. They are mainly due to the dimensional tolerance and surface roughness of the fabrication process.

In Ref. [52], a leaky-wave antenna integrated with an OMT operating in K-band is presented. The antenna consists of a triple-ridge square waveguide perforated on its top wall with crossed slots. The component has been printed by SLA with the propagation axis aligned with the building direction to enhance the good symmetry of the antenna. Then, copper plating was applied. The measurements prove the high precision of the process. In particular, the 3D-printed prototype exhibits a return loss better than 16 dB, port isolation better than 40 dB, and a cross-polarization level below -35 dB.

A K/Ka-band dual-circular polarization antenna feed chain has been reported in Ref. [53]. The device has been designed with an AM-oriented approach. A prototype has been manufactured by SLM with aluminum alloy. The chain is composed of a dual-band orthomode junction (OMJ) which symmetrically extracts the K-band signal while the Ka-band one propagates inline to a series of circular steps connected to a Ka-band septum polarizer. Each of the four arms, where the K-band signal propagates, is integrated with a low-pass filter to isolate the channels from the Ka-band signals. Subsequently, these four arms are recombined in a turnstile junction connected to a K-band septum polarizer. The measured performances of the prototype show very satisfactory performance with values typically required for SATCOM application (i.e., isolation between the bands better than 50 dB, return loss, and isolation between the two polarizations of the same bands than 20 dB).

Finally, a complex RF component is presented in Ref. [54], where a Ku/K-band filter is integrated with an H-plane bend and 90° twist. The conceived geometry makes AM process the only feasible manufacturing technique. The design shows a 70% weight/volume reduction compared to a solution obtained assembling three different parts realized by standard machining. The idea has been stressed by considering the realization of three prototypes with different bend radii to make the device as smaller as possible. Good agreement between measured and simulated RF performance has been achieved even for the prototypes with a bend radius of 30 mm. The three components exhibit a rejection better than 60 dB and an insertion loss better than 0.2 dB. The return loss is better than 25 dB for the prototype with a bend radius of 40 mm, while it is better than 20 dB for the other prototypes.

6. Conclusions

After a brief introduction on the main AM processes, this chapter has summarized the huge work realized by the microwave community on the applicability of AM process on the manufacturing of RF components. For reader convenience, **Table 3**

Technology	Accuracy (μm)	Main frequency range (GHz)
SLM	<100	10–50
SLA	<50	10–90
FDM	100–200	2–20

Table 3.

Accuracy and exploited frequency range of the three AM processes reported in this chapter: SLM, SLA, FDM.

reports the obtained results in terms of accuracy in the relevant frequency range. The most used technology is SLM since it allows the manufacturing of all metal parts. SLA exhibits the best manufacturing accuracy and the largest bandwidth. FDM is used for cheaper components in a low-frequency range, due to the worst manufacturing accuracy. The study/research on AM for microwave components manufacturing is still ongoing, many thematic special sessions are organized within the main conferences in the microwave area. Large margins of improvement are expected in the near future from the manufacturing and design points of view in particular from the integration of different functions in the same realized part.

Conflict of interest

The authors declare no conflict of interest.

Author details

Mauro Lumia¹, Giuseppe Addamo^{1*}, Oscar Antonio Peverini¹, Flaviana Calignano², Giuseppe Virone¹ and Diego Manfredi³


¹ Istituto di Elettronica e di Ingegneria dell'Informazione e delle Telecomunicazioni, National Research Council of Italy, Turin, Italy

² Dipartimento di Ingegneria Gestionale e della Produzione, Politecnico di Torino, Turin, Italy

³ Dipartimento di Scienza Applicata e Tecnologia, Politecnico di Torino, Turin, Italy

*Address all correspondence to: giuseppe.addamo@ieiit.cnr.it

IntechOpen

© 2022 The Author(s). Licensee IntechOpen. This chapter is distributed under the terms of the Creative Commons Attribution License (<http://creativecommons.org/licenses/by/3.0>), which permits unrestricted use, distribution, and reproduction in any medium, provided the original work is properly cited. 

References

- [1] Calignano F, Manfredi D, Ambrosio E, Biamino S, Lombardi M, Atzeni E, et al. Overview on additive manufacturing technologies. *Proceedings of the IEEE*. 2017;**105**: 593-612. DOI: 10.1109/JPROC.2016.2625098
- [2] Gibson I, Stucker B, Rosen DW. *Additive Manufacturing Technologies-Rapid Prototyping*. 1st ed. Boston: Springer; 2010. p. 452. DOI: 10.1007/978-1-4419-1120-9
- [3] Peverini OA, Lumia M, Calignano F, Addamo G, Lorusso M, Ambrosio EP, et al. Selective, laser melting manufacturing of microwave waveguide devices. *Proceedings of the IEEE*. 2017; **105**:620-631. DOI: 10.1109/JPROC.2016.2620148
- [4] Neikov OD, Naboychenko SS, Dowson G. *Handbook of Non-Ferrous Metal Powders*. 1st ed. Amsterdam: Elsevier; 2009. p. 621. DOI: 10.1016/B978-1-85617-422-0.X0001-8
- [5] Spierings AB, Herres N, Levy G. Influence of the particle size distribution on surface quality and mechanical properties in AM steel parts. *Rapid Prototyping Journal*. 2011;**17**: 195-202. DOI: 10.1108/1355254111124770
- [6] Qian M. Metal powder for additive manufacturing. *JOM Journal of the Minerals, Metals and Materials Society*. 2015;**67**:536-537. DOI: 10.1007/s11837-015-1321-z
- [7] Calignano F. Design optimization of supports for overhanging structures in aluminum and titanium alloys by selective laser melting. *Materials and Design*. 2014;**64**:203-213. DOI: 10.1016/j.matdes.2014.07.043
- [8] About Additive manufacturing. Vat Photopolymerization [Internet]. 2021. Available from: <http://www.lboro.ac.uk/research/amrg/> [Accessed: January 31, 2022]
- [9] Peverini OA, Addamo G, Lumia M, Virone G, Calignano F, Lorusso M, et al. Additive manufacturing of Ku/K-band waveguide filters: A comparative analysis among selective-laser melting and stereo-lithography. *IET Microwaves, Antennas and Propagation*. 2017;**11**: 1936-1942. DOI: 10.1049/IET-map.2017.0151
- [10] Khan S, Vahabisani N, Daneshmand M. A fully 3-D printed waveguide and its application as Microfluidically controlled waveguide switch. *IEEE Transactions on Components, Packaging and Manufacturing Technology*. 2017;**7**: 70-80. DOI: 10.1109/TCPMT.2016.2631545
- [11] Coffey M, Verploegh S, Edstaller S, Armstrong S, Grossman E, Popovic Z. Additive manufactured W-band waveguide components. In: 2017 IEEE MTT-S International Microwave Symposium (IMS); 4-9 June 2017; Honolulu, USA. New York: IEEE; 2017. pp. 52-55
- [12] Shen J, Aiken MW, Abbasi M, Parekh DP, Zhao X, Dickey MD, et al. Rapid prototyping of low loss 3D printed waveguides for millimeter-wave applications. In: 2017 IEEE MTT-S International Microwave Symposium (IMS); 4-9 June 2017; Honolulu, USA. New York: IEEE; 2017. pp. 41-44
- [13] Menargues E, Garcia-Vigueras M, Debogovic T, Capdevila S, Dimitriadis AI, de Rijk E, et al. 3D

printed feed-chain and antenna components. In: 2017 IEEE International Symposium on Antennas and Propagation & USNC/URSI National Radio Science Meeting; 9–14 July 2017; San Diego, USA. New York: IEEE; 2017. pp. 1-2

[14] Hollenbeck M, Wamick K, Cathey C, Opra J, Smith R. Selective laser melting aluminum waveguide attenuation at K-band. In: 2017 IEEE MTT-S International Microwave Symposium (IMS); 4–9 June 2017; Honolulu, USA. New York: IEEE; 2017. pp. 45-47

[15] Addamo G, Peverini OA, Lumia M, Virone G, Tascone R, Calignano F, et al. Experimental research activity on additive manufacturing of microwave passive waveguide components. In: 2017 47th European Microwave Conference (EuMC); 10–12 October 2017; Nuremberg, Germany. New York: IEEE; 2017. pp. 496-499

[16] Tomassoni C, Peverini OA, Venanzoni G, Addamo G, Paonessa F, Virone G. 3D printing of microwave and Millimeter-wave filters: Additive manufacturing technologies applied in the development of high-performance filters with novel topologies. *IEEE Microwave Magazine*. 2020;**21**:24-45. DOI: 10.1109/MMM.2020.2979153

[17] Miek D, Simmich S, Höft M. Additive manufacturing of symmetrical X-band waveguide filters for wide-band applications based on extracted pole filter design. In: 2019 IEEE MTT-S International Microwave Workshop Series on Advanced Materials and Processes for RF and THz Applications (IMWS-AMP); 16–18 July 2019; Bochum, Germany. New York: IEEE; 2019. pp. 13-15

[18] Dahle R, Laforge P, Kuhling J. 3-D printed customizable inserts for

waveguide filter design at X-band. *IEEE Microwave and Wireless Components Letters*. 2017;**27**:1080-1082. DOI: 10.1109/LMWC.2017.2754345

[19] Tomassoni C, Venanzoni G, Dionigi M, Sorrentino R. Compact quasi-elliptic filters with mushroom-shaped resonators manufactured with 3-D printer. *IEEE Transactions on Microwave Theory and Techniques*. 2018;**66**:3579-3588. DOI: 10.1109/TMTT.2018.2849067

[20] Tomassoni C, Bozzi M, Dionigi M, Venanzoni G, Perregrini L, Sorrentino R. Additive manufacturing of microwave components: Different approaches and methodologies. In: 2017 International Conference on Electromagnetics in Advanced Applications (ICEAA); 11–15 September 2017; Verona, Italy. New York: IEEE; 2017. pp. 848-851

[21] Salek M, Shang X, Roberts RC, Lancaster MJ, Boettcher F, Weber D, et al. W-band waveguide Bandpass filters fabricated by Micro laser sintering. *IEEE Transactions on Circuits and Systems II: Express Briefs*. 2019;**66**: 61-65. DOI: 10.1109/TCSII.2018.2824898

[22] Zhang F, Gao S, Li J, Yu Y, Guo C, Li S, et al. 3-D printed slotted spherical resonator Bandpass filters with spurious suppression. *IEEE Access*. 2019;**7**: 128026-128034. DOI: 10.1109/ACCESS.2019.2938972

[23] Li J, Guo C, Mao L, Xiang J, Huang G, Yuan T. Monolithically 3-D printed hemispherical resonator waveguide filters with improved out-of-band rejections. *IEEE Access*. 2019;**6**: 57030-57048. DOI: 10.1109/ACCESS.2018.2872696

[24] Périgaud A, Tantot O, Delhote N, Verdeyme S, Bila S, Pacaud D, et al. Continuously tuned Ku-band cavity

- filter based on dielectric Perturbors made by ceramic additive manufacturing for space applications. *Proceedings of the IEEE*. 2017;**105**: 677-687. DOI: 10.1109/JPROC.2017.2663104
- [25] Périgaud A, Tantot O, Delhote N, Verdeyme S, Bila S, Baillargeat D. Bandpass filter based on skeleton-like Monobloc dielectric pucks made by additive manufacturing. In: 2018 48th European Microwave Conference (EuMC); 23–27 September 2018; Madrid, Spain. New York: IEEE; 2018. pp. 296-299
- [26] Addamo G, Peverini OA, Calignano F, Manfredi D, Paonessa F, Virone G, et al. 3-D printing of high-performance feed horns from Ku- to V-bands. *IEEE Antennas and Wireless Propagation Letters*. 2018;**17**:2036-2040. DOI: 10.1109/LAWP.2018.2859828
- [27] Reinhardt A, Möbius-Labinski M, Asmus C, Bauereiss A, Höft M. Additive manufacturing of 300 GHz corrugated horn antennas. In: 2019 IEEE MTT-S International Microwave Workshop Series on Advanced Materials and Processes for RF and THz Applications (IMWS-AMP); 16–18 July 2019; Bochum, Germany. New York: IEEE; 2019. pp. 40-42
- [28] Maas J, Liu B, Hajela S, Huang Y, Gong X, Chappell WJ. Laser-based layer-by-layer polymer Stereolithography for high-frequency applications. *Proceedings of the IEEE*. 2017;**105**: 645-654. DOI: 10.1109/JPROC.2016.2629179
- [29] Teniente J, Iriarte JC, Caballero R, Valcázar D, Goñi M, Martínez A. 3-D printed horn antennas and components performance for space and telecommunications. *IEEE Antennas and Wireless Propagation Letters*. 2018;**17**: 2070-2074. DOI: 10.1109/LAWP.2018.2870098
- [30] Biurrun-Quel C, Lacombe E, Giancesello F, Luxey C, Del-Río C. Characterization of 3D-printed choke horn antenna for 5G backhaul applications. In: 2019 13th European Conference on Antennas and Propagation (EuCAP); 31 March–5 April 2019; Krakow, Poland. New York: IEEE; 2019. pp. 1-4
- [31] Foged LJ, Giacomini A, Morbidini R, Saccardi F, Schirosi V, Boumans M, et al. Investigation of additive manufacturing for broadband choked horns at X/Ku band. *IEEE Antennas and Wireless Propagation Letters*. 2018;**17**:2003-2007. DOI: 10.1109/LAWP.2018.2868611
- [32] Cailloce Y, Hourlay P, Lebrun F, Palacin B. Additive manufacturing of Ku band horn antennas for telecommunications space applications. In: 12th European Conference on Antennas and Propagation (EuCAP); 9–13 April 2018; London, UK. Stevenage: IET; 2018. pp. 1-4
- [33] Chio T, Huang G, Zhou S. Application of direct metal laser sintering to waveguide-based passive microwave components, antennas, and antenna arrays. *Proceedings of the IEEE*. 2016;**105**:632-644. DOI: 10.1109/JPROC.2016.2617870
- [34] Shamvedi D, Danilenkoff C, Karam S, O'Leary P, Raghavendra R. 3D printed periodic structures in a horn antenna for side-lobe reduction using direct metal laser sintering. In: Loughborough Antennas & Propagation Conference (LAPC); 13–14 Nov. 2017; Loughborough, UK. Stevenage: IET; 2017. pp. 1-4
- [35] Zhang S, Cadman D, Vardaxoglou JYC. Additively

manufactured profiled conical horn antenna with dielectric loading. *IEEE Antennas and Wireless Propagation Letters*. 2018;**17**:2128-2132. DOI: 10.1109/LAWP.2018.2871029

[36] Genc A, Basyigit IB, Goksu T, Helhel S. Investigation of the performances of X-Ku band 3D printing pyramidal horn antennas coated with the different metals. In: 2017 10th International Conference on Electrical and Electronics Engineering (ELECO); 30 November–2 December 2017; Bursa, Turkey. New York: IEEE; 2017. pp. 1012-1016

[37] Addamo G, Peverini OA, Virone G, Paonessa F, Manfredi D, Calignano F. 3D printing of Ka band Orthomode transducers. In: 2018 IEEE MTT-S International Microwave Workshop Series on Advanced Materials and Processes for RF and THz Applications (IMWS-AMP); 16–18 July 2018; Ann Arbor, USA. New York: IEEE; 2018. pp. 1-3

[38] Addamo G et al. Additive manufacturing of Ka-band dual-polarization waveguide components. *IEEE Transactions on Microwave Theory and Techniques*. 2018;**66**:3589-3596. DOI: 10.1109/TMTT.2018.2854187

[39] Kilian M, Hartwanger C, Schneider M, Hatzenbichler M. Waveguide components for space applications manufactured by additive manufacturing technology. *IET Microwaves, Antennas and Propagation*. 2017;**11**:1949-1954. DOI: 10.1049/IET-MAP.2016.0984

[40] Booth P, Roberts R, Szymkiewicz M, Hartwanger C. Using additive manufacturing for feed chain and other passive microwave components. In: 2017 11th European Conference on Antennas and Propagation (EUCAP); 19–24 March

2017; Paris, France. New York: IEEE; 2017. pp. 558-562

[41] Kohl P, Kilian M, Schinagl-Weiß A, Hartwanger C. Additive manufacturing developments for satellite antenna applications from C- to Ka-band. In: 2019 12th German Microwave Conference (GeMiC); 25–27 March 2019; Stuttgart, Germany. New York: IEEE; 2019. pp. 222-2250

[42] Addamo G, Peverini OA, Manfredi D, Calignano F, Paonessa F, Lumia M, et al. Electromagnetic and mechanical analyses of a 3D-printed ka-band integrated twist and orthomode transducer. In: 2019 IEEE MTT-S International Microwave Workshop Series on Advanced Materials and Processes for RF and THz Applications (IMWS-AMP); 16–18 July 2019; Bochum, Germany. New York: IEEE; 2019. pp. 31-33

[43] García-Vigueras M, Menargues E, Debogovic T, Silva J, Dimitriadis A, Capdevila S, et al. Mm-wave antennas and components: Profiting from 3D-printing. In: 2017 International Conference on Electromagnetics in Advanced Applications (ICEAA); 11–15 September 2017; Verona, Italy. New York: IEEE; 2017. pp. 1016-1020

[44] Deutschmann B, Jacob AF. Broadband septum polarizer with triangular common port. *IEEE Transactions on Microwave Theory and Techniques*. 2020;**68**:693-700. DOI: 10.1109/TMTT.2019.2951138

[45] Peverini OA, Lumia M, Addamo G, Calignano F, Virone G, Ambrosio EP, et al. Integration of RF functionalities in microwave waveguide components through 3D metal printing. In: 2017 IEEE MTT-S International Microwave Symposium (IMS); 4–9 June 2017;

Honolulu, USA. New York: IEEE; 2017.
pp. 48-51

[46] Borgne FL, Cochet G, Haumant J, Diedhiou D, Donnart K, Manchec A. An integrated Monobloc 3D printed front-end in Ku-band. In: 2019 49th European Microwave Conference (EuMC); 1–3 October 2019; Paris, France. New York: IEEE; 2019. pp. 786-789

[47] Saeidi-Manesh H, Saeedi S, Mirmozafari M, Zhang G, Sigmarsson HH. Design and fabrication of orthogonal-mode transducer using 3-D printing technology. *IEEE Antennas and Wireless Propagation Letters*. 2018; **17**:2013-2016. DOI: 10.1109/LAWP.2018.2847654

[48] Kilian M, Schinagl-Weiß A, Kohl P, Sommer A, Hartwanger C, Schneider M. Additive layer manufactured waveguide RF components. In: 2019 49th European Microwave Conference (EuMC); 1–3 October 2019; Paris, France. New York: IEEE; 2019. pp. 790-793

[49] Kilian M, Schinagl-Weiß A, Sommer A, Hartwanger C, Schneider M. Ku-band SFB-cluster manufactured by additive manufacturing techniques. In: 2019 13th European Conference on Antennas and Propagation (EuCAP); 31 March–5 April 2019; Krakow, Poland. New York: IEEE; 2019. pp. 1-4

[50] Kilian M, Kohl P, Hartwanger C, Schneider M. High gain Ka-band ALM feed chain. In: 2019 IEEE MTT-S International Microwave Workshop Series on Advanced Materials and Processes for RF and THz Applications (IMWS-AMP); 16–18 July 2019; Bochum, Germany. New York: IEEE; 2019. pp. 37-39

[51] Zhang B, Li R, Wu L, Sun H, Guo Y. A highly integrated 3-D printed metallic K-band passive front end as the unit cell

in a large Array for satellite communication. *IEEE Antennas and Wireless Propagation Letters*. 2018; **17**: 2046-2050. DOI: 10.1109/LAWP.2018.2824298

[52] Dorlé A, Gillard R, Menargues E, Van Der Vorst M, De Rijk E, Martín-Iglesias P, et al. Additive manufacturing of modulated triple-ridge leaky-wave antenna. *IEEE Antennas and Wireless Propagation Letters*. 2018; **17**:2123-2127. DOI: 10.1109/LAWP.2018.2848723

[53] Addamo G et al. 3D printing of a monolithic K/Ka-band dual-circular polarization antenna-feeding network. *IEEE Access*. 2021; **9**:88243-88255. DOI: 10.1109/ACCESS.2021.3089826

[54] Peverini OA et al. Integration of an H -plane bend, a twist, and a filter in Ku/K-band through additive manufacturing. *IEEE Transactions on Microwave Theory and Techniques*. 2018; **66**:2210-2219. DOI: 10.1109/TMTT.2018.2809505